

# High ammonia adsorption in MFM-300 materials: dynamics and charge-transfer in host-guest binding

Xue Han,<sup>1†</sup> Wanpeng Lu,<sup>1†</sup> Yinlin Chen,<sup>1</sup> Ivan da Silva,<sup>2</sup> Jiangnan Li,<sup>1</sup> Longfei Lin,<sup>1</sup> Weiyao Li,<sup>1</sup> Alena M. Sheveleva,<sup>1,3</sup> Harry G. W. Godfrey,<sup>1</sup> Zhenzhong Lu,<sup>1</sup> Floriana Tuna,<sup>1,3</sup> Eric J. L. McInnes,<sup>1,3</sup> Yongqiang Cheng,<sup>4</sup> Luke L. Daemen,<sup>4</sup> Laura J. McCormick McPherson<sup>5</sup>, Simon J. Teat<sup>5</sup>, Mark D. Frogley<sup>6</sup>, Svemir Rudic,<sup>2</sup> Pascal Manuel,<sup>2</sup> Anibal J. Ramirez-Cuesta,<sup>4</sup> Sihai Yang<sup>1\*</sup> and Martin Schröder<sup>1\*</sup>

1. Department of Chemistry, University of Manchester, Manchester, M13 9PL, UK

2. ISIS Facility, Science and Technology Facilities Council (STFC), Rutherford Appleton Laboratory, Didcot, OX11 0QX, UK

3. Photon Science Institute, University of Manchester, Manchester, M13 9PL, UK

4. Neutron Scattering Division, Neutron Sciences Directorate, Oak Ridge National Laboratory, Oak Ridge, TN 37831, USA

5. Advanced Light Source, Lawrence Berkeley National Laboratory, Berkeley, CA 94720 (USA)

6. Diamond Light Source, Harwell Science Campus, Oxfordshire, OX11 0DE (UK)

†: Authors contributed equally to this work.

**ABSTRACT:** NH<sub>3</sub> (ammonia) is a promising energy resource owing to its high hydrogen density. However, its widespread application is restricted by the lack of efficient and corrosion-resistant storage materials. Here, we report high NH<sub>3</sub> adsorption in a series of robust metal-organic framework (MOF) materials, MFM-300(M) (M = Fe, V, Cr, In). MFM-300(M) (M = Fe, V<sup>III</sup>, Cr) show fully reversible capacity for >20 cycles, reaching capacities of 16.1, 15.6 and 14.0 mmol g<sup>-1</sup>, respectively, at 273 K and 1 bar. Under the same condition, MFM-300(V<sup>IV</sup>) exhibits the highest uptake among this series of MOFs of 17.3 mmol g<sup>-1</sup>. *In situ* neutron powder diffraction, single crystal X-ray diffraction and electron paramagnetic resonance spectroscopy confirm that the redox-active V centre enables host-guest charge-transfer, with V<sup>IV</sup> being reduced to V<sup>III</sup> and NH<sub>3</sub> oxidised to hydrazine, N<sub>2</sub>H<sub>4</sub>. A combination of *in situ* inelastic neutron scattering and DFT modelling has revealed the binding dynamics of adsorbed NH<sub>3</sub> within these MOFs to afford a comprehensive insight into the application of MOF materials to the adsorption and conversion of NH<sub>3</sub>.

Nearly 200 million tons of NH<sub>3</sub> (ammonia) are produced annually across the world. NH<sub>3</sub> is widely considered as one of the most viable media for hydrogen storage and distribution due to its high volumetric (~0.105 kg/L or 3.6 kWh/L at 25 °C) and gravimetric (17.7 wt.% or 5.8 kWh/kg) hydrogen energy densities<sup>1</sup>. It is also recognized as a renewable fuel which can be produced at scale, at low cost and combusted in fuel cells to yield H<sub>2</sub>O and N<sub>2</sub> as products<sup>2</sup>. These favourable properties make NH<sub>3</sub> a promising potential hydrogen carrier for on-board storage. However, several prerequisites need to be fulfilled for any practical application, including the development of safe and high-capacity storage media, efficient cracking processes, and an effective system for capture and removal of NH<sub>3</sub> that may leak. Even 0.1 ppm NH<sub>3</sub> can poison the proton exchange membranes within fuel cells<sup>3</sup>.

A variety of conventional sorbent materials have been investigated for NH<sub>3</sub> capture and storage, but these tend to show limited

capacities. Examples include resins (11.4 mmol g<sup>-1</sup> in Amberlyst 15<sup>4</sup>), zeolites (9.3 mmol g<sup>-1</sup> in 13X zeolite<sup>5</sup>) and mesoporous silica (8.8 mmol g<sup>-1</sup> in MCM-41<sup>6</sup>). The presence of surface acidic functionalities<sup>7</sup>, especially hydroxyl, carboxyl groups, and open metal sites<sup>8</sup> can significantly enhance NH<sub>3</sub> uptake. Therefore, hybrid MOF materials with high porosity and accessible functional groups have attracted increasing attention for NH<sub>3</sub> adsorption<sup>9</sup>. For example, [Cu<sub>2</sub>Cl<sub>2</sub>(BBTA)] [H<sub>2</sub>BBTA = 1*H*,5*H*-benzo(1,2-*d*:4,5-*d'*)bistriazole] incorporating open metal sites shows an exceptional NH<sub>3</sub> uptake of 19.8 mmol g<sup>-1</sup> at 298 K and 1 bar<sup>10</sup>. [M<sub>2</sub>Cl<sub>2</sub>(BTDD)] (H<sub>2</sub>BTDD = bis(1*H*-1,2,3-triazolo[4,5-*b*],[4',5'-*i*])dibenzo[1,4]dioxin; M = Mn, Co, Ni) with extended linkers also exhibited high and reversible NH<sub>3</sub> uptakes of 15.47, 12.00, and 12.02 mmol/g, respectively, for up to 3 cycles<sup>11</sup>. DUT-6 functionalised with aromatic hydroxyl groups also exhibits a high NH<sub>3</sub> uptake of 16.4 mmol/g at 298 K and 1 bar<sup>12</sup>. However, as with DUT-6 and many

other systems, structural degradation occurs over time due to the highly corrosive nature of  $\text{NH}_3$ , especially at high concentrations, and this often leads to irreversible adsorption<sup>13</sup>. To date, stable MOFs showing reversible and high  $\text{NH}_3$  adsorption remain rare. Additionally, the binding dynamics of adsorbed  $\text{NH}_3$  molecules within MOFs have not been reported to date owing in part to the complexity of the molecular modes of  $\text{NH}_3$ , even at cryogenic temperatures.

The highly stable MOF, MFM-300(Al), exhibits fully reversible adsorption of  $\text{NH}_3$  (15.7 mmol  $\text{g}^{-1}$  at 273 K and 1 bar), and more intriguingly, the packing density of  $\text{NH}_3$  within the pores approaches that of liquid  $\text{NH}_3$ <sup>14</sup>. The stable isostructural analogues MFM-300(M) (M = Fe, Cr, In) can be prepared, in addition to the redox-active MFM-300(M) (M =  $\text{V}^{\text{III}}$ ,  $\text{V}^{\text{IV}}$ )<sup>15</sup>. The rigid scaffold of these MFM-300 materials provides an excellent platform to interrogate the dynamics of adsorbed  $\text{NH}_3$  molecules. We report the systematic study of  $\text{NH}_3$  adsorption in these MOFs by both isotherm and dynamic breakthrough experiments. The preferred binding domains of  $\text{NH}_3$  guest molecules have been determined by *in situ* synchrotron X-ray single crystal diffraction and neutron powder diffraction (NPD). We also report the first investigation of the dynamics of adsorbed  $\text{NH}_3$  molecules within MOFs by *in situ* inelastic neutron scattering (INS) to understand the host-guest binding interactions. MFM-300( $\text{V}^{\text{IV}}$ ) was of particular interest since it not only shows the highest  $\text{NH}_3$  uptake, but also it undergoes a host-guest charge-transfer leading to the oxidation of adsorbed  $\text{NH}_3$  to hydrazine ( $\text{N}_2\text{H}_4$ ) within the pore.

## Results and Discussion

### Analysis of $\text{NH}_3$ adsorption isotherms and breakthrough curves

The  $\text{NH}_3$  adsorption isotherms from 0-1.0 bar between 273 and 323 K were measured for the MFM-300 series under investigation (Figure 1 a-d). The  $\text{NH}_3$  uptakes at 273 K and 1.0 bar were measured as 14.0, 16.1, 15.6 and 17.3 mmol  $\text{g}^{-1}$  for MFM-300(M) (M = Cr, Fe,  $\text{V}^{\text{III}}$ ,  $\text{V}^{\text{IV}}$ ), respectively. These uptake values compare favourably with the leading sorbent materials for  $\text{NH}_3$  in literature (Table S13), and all of the MFM materials show high framework stability and an increase of isothermal uptakes with decreasing temperature (Figure 1). The isosteric heats of adsorption ( $Q_{st}$ ) calculated from these isotherms at different temperatures are in the range of 30-65 kJ  $\text{mol}^{-1}$  (Table 1). Notably though, MFM-300(In) shows significant loss of  $\text{NH}_3$  capacity over repeated cycles (Figure S1), and is unstable under these conditions.

MFM-300(M) (M = Cr, Fe,  $\text{V}^{\text{III}}$ ) all display reversible uptake of  $\text{NH}_3$  with consistent adsorption capacities over 20 cycles of adsorption/desorption of  $\text{NH}_3$  under pressure-

swing conditions. The residual amount of  $\text{NH}_3$  left in MFM-300(M) (M = Cr, Fe,  $\text{V}^{\text{III}}$ ) on degassing is ~9% , but this can be readily desorbed by heating at 333 K for 2 h (Figure 1e-h). In contrast, MFM-300 ( $\text{V}^{\text{IV}}$ ) shows a hysteresis loop, characteristic of capillary condensation in mesopores and/or due to a broad distribution of pore size and shape<sup>16</sup> (Figure 1a-d). Considering the pore size (~6.7 x 6.7  $\text{\AA}^2$ ) of MFM-300( $\text{V}^{\text{IV}}$ ), this result suggests a specific and potentially strong host-guest binding upon the adsorption of  $\text{NH}_3$  in this material. MFM-300( $\text{V}^{\text{IV}}$ ) also exhibits an intriguing *increase* of both capacity and residue within the first 18 cycles. The residual amount of  $\text{NH}_3$  left within MFM-300( $\text{V}^{\text{IV}}$ ) upon regeneration by pressure-swing steadily increases from 8 to 20% along these cycles indicating an accumulation of strongly-bound  $\text{NH}_3$ -derived species in MFM-300( $\text{V}^{\text{IV}}$ ), which cannot be desorbed by reducing pressure alone. This residue can be removed by heating under dynamic vacuum, but some structural degradation of the MOF also occurs. Interestingly, the regenerable component of the  $\text{NH}_3$  sorption capacity of MFM-300( $\text{V}^{\text{IV}}$ ) remains unchanged over cycles, indicating that the accumulated residue derived from  $\text{NH}_3$  does not adversely affect the sorbent capacity; the structural integrity of MFM-300( $\text{V}^{\text{IV}}$ ) after these cycles is confirmed by powder X-ray diffraction (PXRD) (Figure 1i).

The ability of these MOFs to capture  $\text{NH}_3$  at low concentration (1000 ppm) was confirmed by dynamic breakthrough experiments (Figure 1j) at 298 K. The dynamic  $\text{NH}_3$  uptake calculated from these breakthrough curves are 1.1, 0.6, 1.9 and 1.0 mmol  $\text{g}^{-1}$  for MFM-300(M) (M = Cr, Fe,  $\text{V}^{\text{III}}$ , and  $\text{V}^{\text{IV}}$ ), respectively. While MFM-300( $\text{V}^{\text{IV}}$ ) exhibits the highest isothermal uptake, MFM-300( $\text{V}^{\text{III}}$ ) demonstrates the maximum retention of  $\text{NH}_3$  under dynamic conditions. The discrepancy between isothermal and dynamic uptake is widely acknowledged,<sup>17</sup> as the nature of these two types of experiments is fundamentally different. Breakthrough experiments are undertaken at the ppm level of  $\text{NH}_3$  under flow conditions, whereas isotherms were measured statically with pure  $\text{NH}_3$ . Kinetic and thermodynamic factors therefore need to be taken into account in such experiments.

### Determination of preferred binding domains of $\text{ND}_3$

Neutron powder diffraction (NPD) data for  $\text{ND}_3$ -loaded MFM-300 were collected at 10 K (ratio of  $\text{ND}_3$ : M = 0.3, 0.5, 2.2, 2.2 for M = In,  $\text{V}^{\text{III}}$ , Fe,  $\text{V}^{\text{IV}}$ , respectively). Notwithstanding its low stability to  $\text{NH}_3$ , NPD confirmed that MFM-300(In) retains its structure at low loadings of  $\text{ND}_3$ , and Rietveld refinement of these data illustrated distinct binding sites for  $\text{ND}_3$  (Figure 2). Two binding sites for  $\text{ND}_3$  are found in MFM-300(M) (M = In,  $\text{V}^{\text{III}}$ ) and an additional site for  $\text{ND}_3$  was located in MFM-

300(Fe) due to the higher ND<sub>3</sub> loading in this latter experiment. Site I has the highest occupancy with hydrogen bonding between the O<sub>bridge</sub>-H $\cdots$ ND<sub>3</sub> (1.411-1.978 Å) involving the bridging hydroxyl groups of the MOF. This is supplemented by further hydrogen bonding (H<sub>aromatic</sub> $\cdots$ ND<sub>3</sub> = 2.738-3.174 Å; ND<sub>3</sub> $\cdots$ O<sub>ligand</sub> = 3.078-3.179 Å) and electrostatic interactions (ND<sub>3</sub> $\cdots$ aromatic rings = 2.946-3.132 Å).

Hydrogen/deuterium site exchange is also observed between the adsorbed ND<sub>3</sub> and the H-O<sub>bridge</sub> group on the framework MFM-300(M) (M = In, Fe, V<sup>III</sup>), which is similar to that observed in ND<sub>3</sub>-loaded MFM-300(Al)<sup>[14]</sup>. Site II is located further towards the centre of the pore and is anchored in place through hydrogen bonding interactions (ND<sub>3</sub> $\cdots$ O<sub>ligand</sub> = 2.284-3.065 Å). Site III in MFM-300(Fe) is primarily stabilised by electrostatic interactions (ND<sub>3</sub> $\cdots$  aromatic rings = 3.146 Å). In MFM-300(Fe), intermolecular hydrogen bonds between ND<sub>3</sub> molecules (2.327-3.193 Å) were also observed, and these propagate along the 1D channel to form a cooperative {ND<sub>3</sub>}<sub>∞</sub> network. These multiple interactions between molecules of ND<sub>3</sub> are similar to those observed in solid ND<sub>3</sub> at 2 K (N $\cdots$ D = 2.357 Å)<sup>18</sup>.

MFM-300(V<sup>IV</sup>) does not incorporate bridging hydroxyl groups but rather has bridging oxo centres to balance the charge of the oxidised V centre.<sup>15</sup> Thus, hydrogen bonding to hydroxyl groups as above is not possible and the guest molecules are located towards the centre of the pore. Interestingly, unlike MFM-300(M) (M = In, Fe, V<sup>III</sup>), where adsorbed ND<sub>3</sub> molecules remain chemically intact in the pore, in MFM-300(V<sup>IV</sup>) a molecule of N<sub>2</sub>D<sub>4</sub> molecule is identified at site II with an ND<sub>3</sub> molecule at site I being partially protonated to ND<sub>4</sub><sup>+</sup>. The bridging oxo centres remain unprotonated. Both sites are stabilised through hydrogen bonding (ND<sub>3</sub> $\cdots$ O<sub>ligand</sub> = 2.529-3.092 Å) and the amount of N<sub>2</sub>D<sub>4</sub> at site II is calculated to be 0.5 N<sub>2</sub>H<sub>4</sub> per V centre, consistent with the redox equilibrium based upon a complete reduction of V<sup>IV</sup> to V<sup>III</sup> centres.

### Studies of host-guest charge transfer

The oxidation state of the V centers in MFM-300(V<sup>IV</sup>) before and after NH<sub>3</sub> adsorption was investigated by X-band (9.86 GHz) electron paramagnetic resonance (EPR) at room temperature (Figure 3a). In six-coordinate O<sub>h</sub> symmetry, the d<sup>2</sup> V<sup>III</sup> centre has a triplet ground state (<sup>3</sup>T<sub>1g</sub>). Lower symmetry removes orbital degeneracy resulting in a singlet ground state with S = 1, where spin-orbit coupling leads to a large zero-field splitting (up to tens of cm<sup>-1</sup>). Therefore, most V<sup>III</sup> species are EPR-silent at X-band frequencies, which is also the case for MFM-300(V<sup>III</sup>). Bare MFM-300(V<sup>IV</sup>) however shows a single resonance centred at g = 1.955, consistent with a d<sup>1</sup> V<sup>IV</sup> centre, and a broad

peak-to-peak linewidth is measured at ca. 130 G due to the exchange interactions in the V<sup>IV</sup> centre. Upon loading of NH<sub>3</sub>, this signal decreases significantly, suggesting the reduction of V<sup>IV</sup> to V<sup>III</sup> centres in MFM-300(V<sup>IV</sup>). Thus, the redox activity of MFM-300(V<sup>IV</sup>) promotes a host-guest charge-transfer between the MOF and the adsorbed ND<sub>3</sub> molecules, resulting in the reduction of V<sup>IV</sup> centers and concomitant oxidation of NH<sub>3</sub> to N<sub>2</sub>H<sub>4</sub>. Interestingly, the N<sub>2</sub>H<sub>4</sub> molecules can be removed from the pores by soaking the NH<sub>3</sub>-saturated MFM-300(V) in water as confirmed by the Watt and Chrisp method<sup>19</sup>, where a characteristic UV-vis absorption band at 460 nm was observed for the filtrate (see SI).

To gain further insights into the host-guest charge-transfer in MFM-300(V), we sought to monitor directly the change of oxidation state of V centres by bond valence sum (BVS) calculations. Because V is almost transparent in neutron diffraction, a series of *in situ* synchrotron X-ray single-crystal diffraction experiments of MFM-300(M) (M = V<sup>III</sup>, V<sup>IV</sup>) were collected at different NH<sub>3</sub> loadings (Figure 4). As expected, little change in the oxidation state of the V centre (3.05-3.10) was observed for MFM-300(V<sup>III</sup>) upon loading with NH<sub>3</sub> (Table S6, Figure S10-S14). Bare MFM-300(V<sup>IV</sup>) exhibits an oxidation state of 3.70 for the V centre, and no substantial change was observed at low NH<sub>3</sub> loadings (3.70, 3.67 and 3.62 for VC<sub>8</sub>O<sub>5</sub>H<sub>3</sub>·0.2NH<sub>3</sub>, VC<sub>8</sub>O<sub>5</sub>H<sub>3</sub>·1.1NH<sub>3</sub> and VC<sub>8</sub>O<sub>5</sub>H<sub>3</sub>·2.5NH<sub>3</sub>, respectively, Table S7), consistent with the absence of N<sub>2</sub>H<sub>4</sub> molecules in the pore. However, when the loading is increased to VC<sub>8</sub>O<sub>5</sub>H<sub>3</sub>·3.9NH<sub>3</sub>, the oxidation state of the V centre exhibits an apparent drop to 3.52, and simultaneously a molecule of N<sub>2</sub>H<sub>4</sub> is observed as the occupancy of N at site III (H is invisible) exceeded 0.5 [N $\cdots$ N = 1.61(9) Å, 1.56(14) Å]. These results suggest that the charge-transfer between adsorbed NH<sub>3</sub> molecules and the V<sup>IV</sup> centre can only occur when the loading of NH<sub>3</sub> is sufficiently high so that a predominant occupancy of the N site, which is located close to the metal chain, is reached to initiate the redox reaction. Interestingly, this N site {site I in dataset VC<sub>8</sub>O<sub>5</sub>H<sub>3</sub>·0.3NH<sub>3</sub>-regenerate (Figure S21)} is preserved after the sample was degassed under dynamic vacuum at 298 K for 2 h, corresponding to a residual of approximately 7.5% of the adsorption capacity. This is in excellent agreement with that (~8%) observed in the pressure-swing experiment.

### Analysis of host-guest binding dynamics

Combined INS and DFT have been employed to interpret the dynamics of adsorbed NH<sub>3</sub> molecules within MFM-300(M) (M = Al, Fe, V<sup>III</sup>, V<sup>IV</sup>). Vibrational features of both the NH<sub>3</sub> guests and the framework host were successfully captured and assigned based upon DFT calculations using the structural models derived from NPD analyses.

Excellent agreement between experimental and simulated INS spectra were observed for MFM-300(M) (M = Al, Fe, V<sup>III</sup>) (Figure 5). MFM-300(V<sup>IV</sup>) exhibits broad INS features that show discrepancies compared with the simulated INS spectra because of the complex and disordered arrangement of NH<sub>3</sub>, NH<sub>4</sub><sup>+</sup> and N<sub>2</sub>H<sub>4</sub> within the pore, and these had to be simplified within the DFT calculations, which cannot consider the presence of hopping of H centers between sites. This, however, is consistent with the reactive adsorption of NH<sub>3</sub> and the host-guest charge-transfer process that takes place in MFM-300(V<sup>IV</sup>) with NH<sub>3</sub>. Distinct peaks are observed in the INS difference spectra obtained by subtracting the features of the bare MOF and sample cell from the spectra of NH<sub>3</sub>-loaded MOF. Peaks in the low energy region (below 60 meV) are primarily due to the vibrational modes of adsorbed NH<sub>3</sub> molecules, with a small contribution due to changes in the lattice modes of the framework. The features in the higher energy region (80-200 meV) mainly reflect the modes of the framework.

At a loading of 1NH<sub>3</sub> per Al centre in NH<sub>3</sub>@MFM-300(Al), peak I at 6.2 meV represents the translational motion of NH<sub>3</sub> along directions perpendicular to the N...H-O<sub>bridging</sub> bond, whereas peak II at 13.8 meV is due to the translational motion along the direction of the N...H-O<sub>bridging</sub> bond (Figure 5a, b). Peaks III-V (16.1, 19.8, 22.3 meV, respectively) are due to the librational (torsional) motion of NH<sub>3</sub> around its C<sub>3</sub> axis, as well as translational-torsional hybrid motions. Peaks VI-VII at higher energy (34.0, 40.1 meV, respectively) originate from the rocking motions of NH<sub>3</sub> around the N center. When comparing this spectrum to that of the solid NH<sub>3</sub> (translational modes: 8.7-21.0 meV; librational modes: 29.4-32.3 meV; rocking modes: 39.3-54.4 meV), a red-shift of all peaks in the three regions was observed for the adsorbed NH<sub>3</sub> molecules. This reflects the local environment of the adsorbed NH<sub>3</sub> which interacts to the hydroxyl group in the framework via hydrogen bonding, in contrast to the extensive 3D hydrogen bonding network formed between 6 adjacent NH<sub>3</sub> molecules in its solid-state structure. The former affords greater flexibility to the adsorbed NH<sub>3</sub> molecules, whereas the latter imposes more restrictions to intermolecular motions. Another observation is that the INS peaks for the adsorbed NH<sub>3</sub> molecules are broader than those in the pure solid phase, most notably for the translational and librational region. This can be attributed to the isolated environment for the adsorbed molecules causing uncorrelated vibrations of individual NH<sub>3</sub>. In contrast, in crystalline NH<sub>3</sub> the molecules are strongly restrained and vibrate in phase, giving sharp and distinct peaks on the INS spectrum.

INS peaks observed MFM-300(Al) at (i) 87.6, (ii) 114, (iii) 118 and (iv) 143 meV can be assigned to H-C out-of-C<sub>6</sub> plane deformation (in phase along ring, meaning H atoms move in the same

direction), H-C out-of-C<sub>6</sub> plane deformation (anti-phase along ring, meaning neighbouring H atoms move in opposite directions), H-O in V-O-V-plane bending and H-C in-C<sub>6</sub>-plane bending modes, respectively (Figure 5c, e). Upon adsorption of NH<sub>3</sub> into the framework, peak (i) shifts slightly to higher energy, indicating a stiffening effect of the phenyl rings due to the interaction with NH<sub>3</sub>, whereas peak (iv) retains its position and exhibits an intensity change only, suggesting these modes are weakly affected by the NH<sub>3</sub> molecules. The effect of NH<sub>3</sub> upon peak (ii) is phase-dependent, where the mode that involves more displacement of β-H is affected more strongly due to the shorter distance between the NH<sub>3</sub> to β-H than that of the α-H. Overall, the INS analysis is in excellent agreement with the crystal structures determined from NPD experiments and demonstrates that the adsorbed NH<sub>3</sub> molecules interact primarily with the H centers of hydroxyl groups and the C<sub>6</sub> ring at the β position. Detailed spectral interpretations of MFM-300(M) (M = Fe, V<sup>III</sup>, V<sup>IV</sup>) on loading with NH<sub>3</sub> loading are discussed in the SI (Figure S22-S24, Table S10-S12).

Single crystals of MFM-300(M) (M = Fe, V<sup>III</sup>, V<sup>IV</sup>) have been examined further by *in situ* synchrotron FTIR micro-spectroscopy at various NH<sub>3</sub> partial pressures in a flow cell. MFM-300(V<sup>III</sup>) shows that the characteristic O-H stretching mode of the bridging hydroxyl group at 3642 cm<sup>-1</sup>, and the N-H stretching mode (3300-3400 cm<sup>-1</sup>) of adsorbed NH<sub>3</sub> molecules increase steadily with increasing NH<sub>3</sub> loading (Figure 3b). In contrast, bare MFM-300(V<sup>IV</sup>) displays no adsorption bands above 3600 cm<sup>-1</sup> due to the absence of the bridging hydroxyl moiety (Figure 3c). The N-H stretching mode of NH<sub>3</sub> at 3374 cm<sup>-1</sup> grows with the increase of NH<sub>3</sub> partial pressure. Simultaneously, FTIR bands at 970 cm<sup>-1</sup>, 3160 cm<sup>-1</sup> and 3210 cm<sup>-1</sup>, assigned to -NH<sub>2</sub> rocking, -NH<sub>2</sub> symmetrical stretching, and -NH<sub>2</sub> anti-symmetrical stretching of N<sub>2</sub>H<sub>4</sub>, respectively,<sup>[20]</sup> are observed with increasing absorbance as the loading of NH<sub>3</sub> increases. Moreover, these bands assigned to N<sub>2</sub>H<sub>4</sub> remain on treating the material under dynamic vacuum at room temperature, consistent with the residual uptake that was observed in the adsorption and crystallographic experiments.

## Conclusions

Powerful drivers exist for the development of functional materials for NH<sub>3</sub> storage. This work presents a comprehensive study of NH<sub>3</sub> adsorption in porous MFM-300 sorbents. MFM-300(M) (M = Al, Cr, Fe, V<sup>III</sup>, V<sup>IV</sup>) show excellent reversible uptake capacity for NH<sub>3</sub> coupled with high framework stability with great potential for NH<sub>3</sub> capture and storage. Interestingly, the redox-active MFM-300(V<sup>IV</sup>) drives the oxidation of adsorbed NH<sub>3</sub> to N<sub>2</sub>H<sub>4</sub>, which is accompanied by reduction of V<sup>IV</sup> to V<sup>III</sup>, and promotes the NH<sub>3</sub>

adsorption uptake up to 17.3 mmol g<sup>-1</sup>. Combined INS and DFT studies have afforded an in-depth analysis of the binding dynamics of NH<sub>3</sub> in these materials. This study will inspire the future development of porous materials with an integrated function for the storage, capture and conversion for NH<sub>3</sub>.

## ASSOCIATED CONTENT

**Supporting Information.** Supporting Information includes additional experimental details, adsorption isotherm and uptake data, powder X-ray and neutron diffraction data, views of crystal structures, CIF files, EPR and FTIR spectroscopy, INS data, and details for detection of N<sub>2</sub>H<sub>4</sub>. This material is available free of charge via the Internet at <http://pubs.acs.org>.

## AUTHOR INFORMATION

### Corresponding Author

\*Sihai.Yang@manchester.ac.uk  
\*M.Schroder@manchester.ac.uk

### Author Contributions

<sup>†</sup>X. Han and W. Lu contributed equally.

### Notes

The authors declare no competing financial interests.

## ACKNOWLEDGMENT

We thank EPSRC (EP/I011870), the Royal Society and University of Manchester. This project has received funding from the European Research Council (ERC) under the European Union's Horizon 2020 research and innovation programme (grant agreement No 742401, NANO-CHEM). We are grateful to Diamond Light Source and STFC/ISIS Facility for access to Beamlines B22 and TOSCA/WISH, respectively, and to Oak Ridge National Laboratory for access to the VISION spectrometer at the Spallation Neutron Source. This research used resources of Beamlines 11.3.1 and 12.2.1 at the Advanced Light Source, which is a DOE Office of Science User Facility under contract no. DE-AC02-05CH11231. The computing resources were made available through the VirtuES and the ICE-MAN projects, funded by Laboratory Directed Research and Development program and Compute and Data Environment for Science (CADES) at ORNL. J.L. thanks China Scholarship Council (CSC) for funding. AMS is supported by a Royal Society Newton Fellowship.

## REFERENCES

[1] Dong, B. X.; Tian, H.; Wu, Y. C.; Bu, F. Y.; Liu, W. L.; Teng, Y. L.; Diao, G. W. Improved electrolysis of liquid ammonia for hydrogen generation via ammonium salt electrolyte and Pt/Rh/Ir electrocatalysts. *Int. J. Hydrog. Energy*. **2016**, *41*, 14507-14518.  
[2] MacFarlane, D. R.; Cherepanov, P. V.; Choi, J.; Suryanto, B. H.; Hodgetts, R. Y.; Bakker, J. M.; Ferrero Vallana, F. M.; Simonov, A. N. A roadmap to the ammonia economy. *Joule*. **2020**, *4*, 1186-1205.  
[3] Uribe, F.; Brosha, E.; Garzon, F.; Mikkola, M.; Pivovar, B.; Rockward, T.; Valerio, J.; Wilson, M. VII. I. 4

Effect of fuel and air impurities on PEM fuel cell performance. *Hydrog. energy. gov*. **2005**, 1046-1051.

[4] Helminen, J.; Helenius, J.; Paatero, E.; Turunen, I. Adsorption equilibria of ammonia gas on inorganic and organic sorbents at 298.15 K. *J. Chem. Eng.* **2001**, *46*, 391-399.

[5] Helminen, J.; Helenius, J.; Paatero, E.; Turunen, I. Comparison of sorbents and isotherm models for NH<sub>3</sub>-gas separation by adsorption. *AIChE J.* **2000**, *46*, 1541-1555.

[6] Furtado, A. M.; Wang, Y.; Glover, T. G.; LeVan, M. D. MCM-41 impregnated with active metal sites: synthesis, characterization, and ammonia adsorption. *Micropor Mesopor Mat.* **2011**, *142*, 730-739.

[7] Mochizuki, T.; Kubota, M.; Matsuda, H.; Camacho, L. F. E. Adsorption behaviors of ammonia and hydrogen sulfide on activated carbon prepared from petroleum coke by KOH chemical activation. *Fuel Process. Technol.* **2016**, *144*, 164-169.

[8] Yang, Y.; Faheem, M.; Wang, L.; Meng, Q.; Sha, H.; Yang, N.; Yuan, Y.; Zhu, G. Surface pore engineering of covalent organic frameworks for ammonia capture through synergistic multivariate and open metal site Approaches. *Cent. Sci.* **2018**, *4*, 748-754.

[9] (a) Vikrant, K.; Kumar, V.; Kim, K. H.; Kukkar, D. Metal-organic frameworks (MOFs): potential and challenges for capture and abatement of ammonia. *J. Mater. Chem. A*. **2017**, *5*, 22877-22896. (b) Kim, K. C.; Yu, D.; Snurr, R. Q. Computational screening of functional groups for ammonia capture in metal-organic frameworks. *Langmuir*. **2013**, *29*, 1446-1456. (c) Chen, Y.; Zhang, X.; Ma, K.; Chen, Z.; Wang, X.; Knapp, J.; Alayoglu, S.; Wang, F.; Xia, Q.; Li, Z.; Islamoglu, T.; Farha, O. K. A zirconium-based metal-organic framework with 9-connected nodes for ammonia capture. *ACS Appl. Nano Mater.* **2019**, *2*, 6098-6102.

[10] Rieth, A. J.; Dincă, M. Controlled gas uptake in metal-organic frameworks with record ammonia sorption. *J. Am. Chem. Soc.* **2018**, *140*, 3461-3466.

[11] Rieth, A. J.; Tulchinsky, Y.; Dincă, M. High and reversible ammonia uptake in mesoporous azolate metal-organic frameworks with open Mn, Co, and Ni sites. *J. Am. Chem. Soc.* **2016**, *138*, 9401-9404.

[12] Spanopoulos, I.; Xydias, P.; Malliakas, C. D.; Trikalitis, P. N. A straight forward route for the development of metal-organic frameworks functionalized with aromatic -OH groups: synthesis, characterization, and gas (N<sub>2</sub>, Ar, H<sub>2</sub>, CO<sub>2</sub>, CH<sub>4</sub>, NH<sub>3</sub>) sorption properties. *Inorg. Chem.* **2013**, *52*, 855-862.

[13] (a) Katz, M. J.; Howarth, A. J.; Moghadam, P. Z.; DeCoste, J. B.; Snurr, R. Q.; Hupp, J. T.; Farha, O. K. High volumetric uptake of ammonia using Cu-MOF-74/Cu-CPO-27. *Dalton Trans.* **2016**, *45*, 4150-4153. (b) Shustova, N. B.; Cozzolino, A. F.; Reineke, S.; Baldo, M.; Dincă, M. Selective turn-on ammonia sensing enabled by high-temperature fluorescence in metal-organic frameworks with open metal sites. *J. Am. Chem. Soc.* **2013**, *135*, 13326-13329.

[14] Godfrey, H. G.; Da Silva, I.; Briggs, L.; Carter, J. H.; Morris, C. G.; Savage, M.; Dr. Timothy L. Easun; Manuel, P.; Murray, C. A.; Tang, C. C.; Frogley, M.; Cinque, G.; Yang, S.; Schröder, M. Ammonia storage by reversible host-guest site exchange in a robust metal-organic framework. *Angew. Chem. Int. Ed.* **2018**, *57*, 14778-14781.

[15] (a) Lu, Z.; Godfrey, H. G.; Da Silva, I.; Cheng, Y.; Savage, M.; Tuna, F.; McInnes, E. J. L.; Teat, S. J.; Gagnon, K. J.; Frogley, M. D.; Manuel, P.; Rudić, S.; Ramirez-Cuesta, A. J.; Easun, T. L.; Yang, S.; Schröder, M. Modulating supramolecular binding of carbon dioxide in

a redox-active porous metal-organic framework. *Nat. Commun.* **2017**, *8*, 1-10; (b) Han, X.; Hong, Y.; Ma, Y.; Lu, W.; Li, J.; Lin, L.; Sheveleva, A. M.; Tuna, F.; McInnes, E. J. L.; Dejoie, C.; Sun, J.; Yang, S.; Schröder, M. Adsorption of nitrogen dioxide in a redox active vanadium metal-organic framework material. *J. Am. Chem. Soc.*, **2020**, *142*, 15235-15239.

[16] Sing, K. S. Reporting physisorption data for gas/solid systems with special reference to the determination of surface area and porosity. *Pure Appl. Chem.* **1985**, *57*, 603-619.

[17] (a) Han, X.; Yang, S.; Schröder, M. Porous metal-organic frameworks as emerging sorbents for clean air. *Nat. Rev. Chem.* **2019**, *3*, 108-118; (b) Sabouni, R.; Kazemian, H.; Rohani, S. Mathematical modeling and experimental breakthrough curves of carbon dioxide adsorption on metal organic framework CPM-5. *Environ. Sci. Technol.* **2013**, *47*, 9372-9380; (c) Bozbiyik, B.; Assche, T. V.; Lannoeye, J.; De Vos, D. E.; Baron, G. V.; Denayer, J. F. M. Stepped water isotherm and breakthrough curves on aluminium fumarate metal-organic framework: experimental and modelling study. *Adsorption*. **2017**, *23*, 185-192.

[18] Hewat, A. W.; Riekkel, C. The crystal structure of deuteroammonia between 2 and 180 K by neutron powder profile refinement. *Acta Crystallogr. A.* **1979**, *35*, 569-571.

[19] Gamble, D. S.; Hoffman, I. Photometric analysis of trace amounts of hydrazine with p-

dimethylaminobenzaldehyde. *Can. J. Chem.* **1967**, *45*, 2813-2819.

[20] Dirtu, D.; Odochian, L.; Pui, A.; Humelnicu, I. Thermal decomposition of ammonia. N<sub>2</sub>H<sub>4</sub>-an intermediate reaction product. *Open Chem. J.* **2006**, *4*, 666-673.

**Figure 1.** (a)-(d) Adsorption isotherms for NH<sub>3</sub> in MFM-300(M) (M = Cr, Fe, V<sup>III</sup>, V<sup>IV</sup>) at 273-328 K (adsorption: solid; desorption: open symbols). (e)-(h) Cyclic adsorption-desorption of NH<sub>3</sub> in MFM-300(M) (M = (Cr, Fe, V<sup>III</sup>, V<sup>IV</sup>) at 298 K between 0-0.15 bar, dark-coloured bars show the residual NH<sub>3</sub> left within the MOF after desorption under dynamic vacuum at 298 K. (i) PXRD patterns of as-synthesised MFM-300 and the samples after a cycle of adsorption and desorption of NH<sub>3</sub>. (j) Breakthrough curves for NH<sub>3</sub> (1000 ppm diluted in He) through fixed beds packed with samples of MFM-300 samples at 298 K at 1.0 bar.

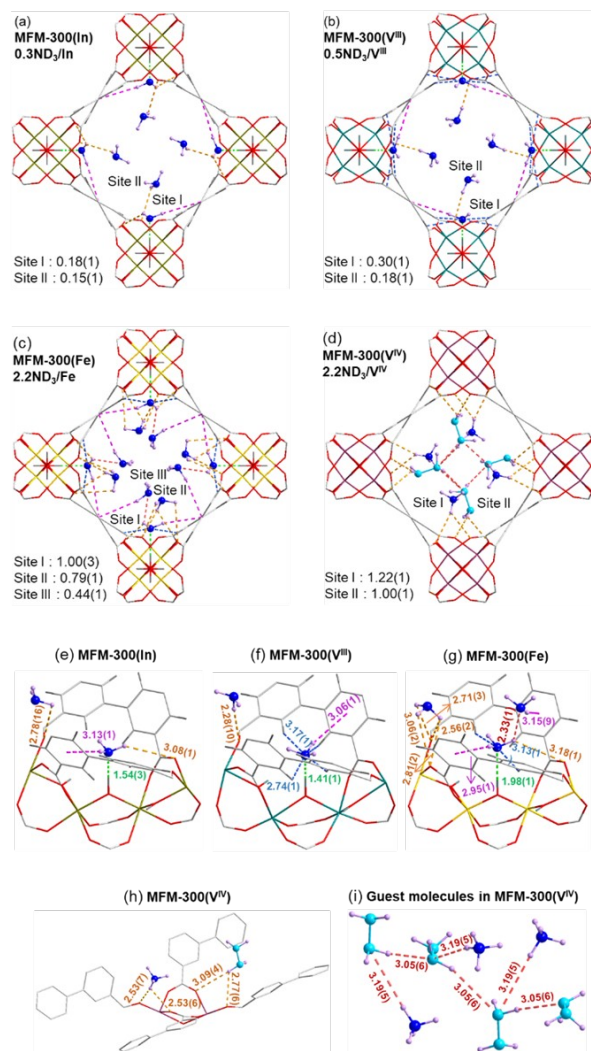
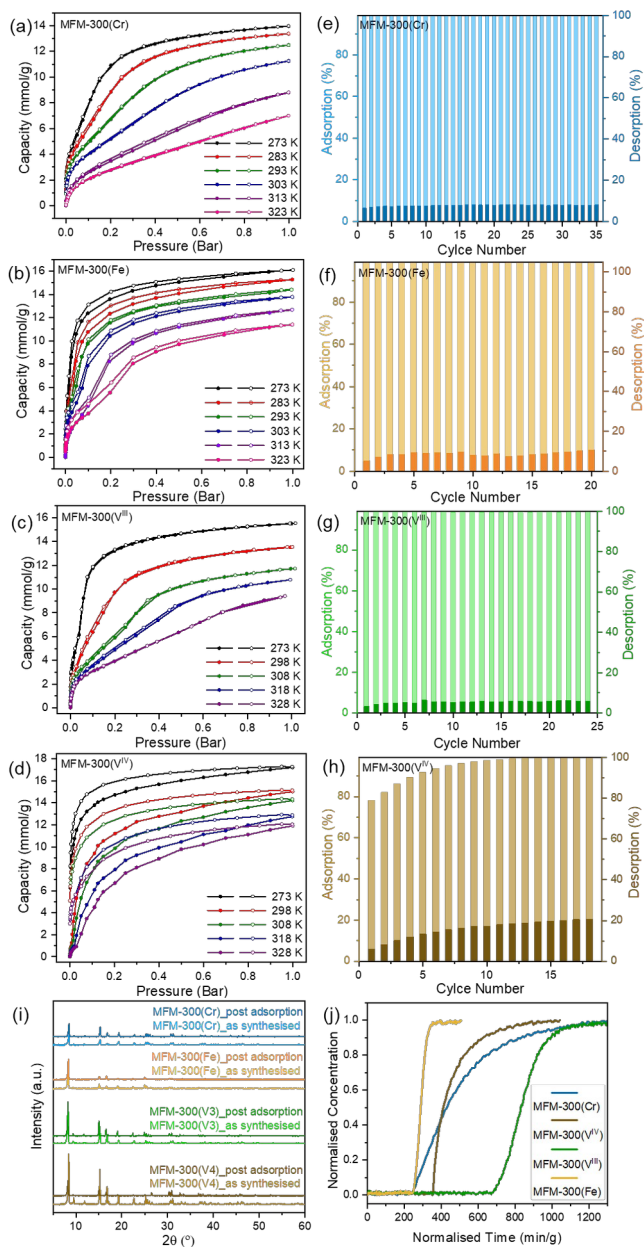


**Figure 2.** Views of sites for  $\text{ND}_3$  in MFM-300(M) (M = In,  $\text{V}^{\text{III}}$ , Fe,  $\text{V}^{\text{IV}}$ ) determined by neutron powder diffraction at 10 K. The occupancy of each site has been converted into  $\text{ND}_3/\text{M}$  for clarity. (a)-(d): Views along  $c$ -axis showing packing of the guest molecules within the pore. (e)-(h): Views of detailed host-guest interactions. (i): Cooperative network composed of  $\text{N}_2\text{D}_4$  (N atoms: light blue) and  $\text{ND}_4^+$  (N atoms: dark blue) in MFM-300(V). In: dark yellow;  $\text{V}^{\text{III}}$ : green; Fe: yellow;  $\text{V}^{\text{IV}}$ : magenta; O: red; C: white; H: grey; N: blue; D: purple.

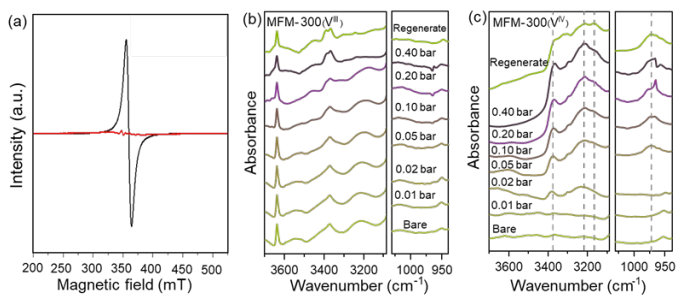


**Figure 3.** (a) X-band (9.87 GHz) EPR spectra of bare and  $\text{NH}_3$ -loaded MFM-300( $\text{V}^{\text{IV}}$ ). *In situ* synchrotron FTIR spectra for single-crystals of (b) MFM-300( $\text{V}^{\text{III}}$ ) and (c) MFM-300( $\text{V}^{\text{IV}}$ ) at various partial pressures of  $\text{NH}_3$  (diluted in dry  $\text{N}_2$ ) and after regeneration under a dry  $\text{N}_2$  flow at 100  $\text{mL min}^{-1}$  at 298 K for 2 hour.

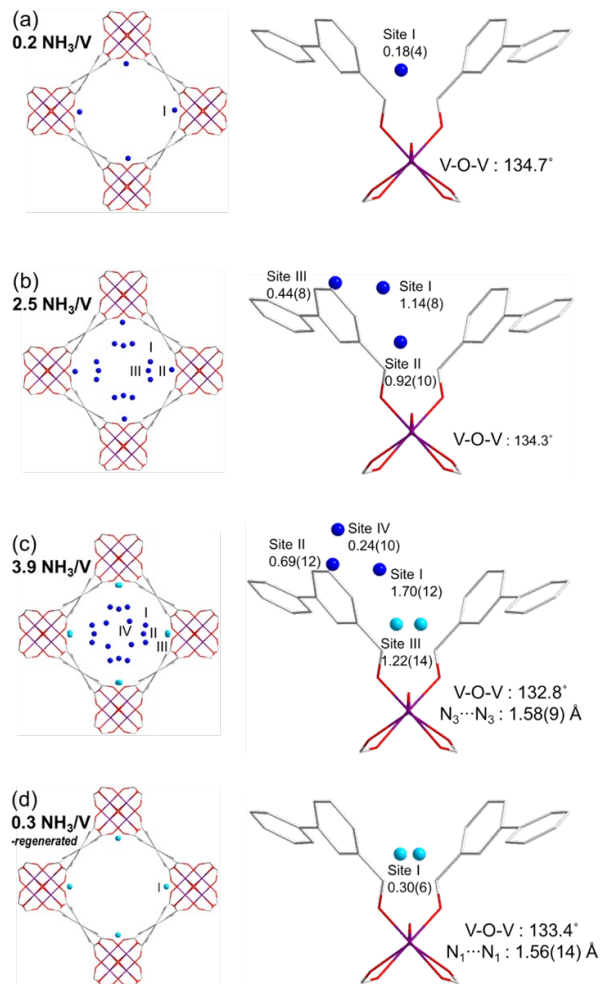


**Figure 4.** Views of single crystal X-ray structures of  $\text{NH}_3$ -loaded MFM-300( $\text{V}^{\text{IV}}$ ) along the  $c$ -axis (V: magenta; O: red; C: white; H: grey; N: light blue for  $\text{N}_2\text{H}_4$ , dark blue for  $\text{NH}_3$  and  $\text{NH}_4^+$ ). The structures were obtained from *in situ* synchrotron X-ray single crystal diffraction at 273 K, and the occupancy of

each site has been converted to  $\text{NH}_3/\text{V}^{\text{IV}}$  for clarity. (a)-(c) show the structure with increasing loading of  $\text{NH}_3$  from 0.2  $\text{NH}_3/\text{V}$  to 3.9  $\text{NH}_3/\text{V}$ , and (d) shows the structure after the sample being degassed under dynamic vacuum at 298 K for 2h.  $\text{N}_2\text{H}_4$  (N atoms: light blue) and  $\text{NH}_3$  (N atoms: dark blue).

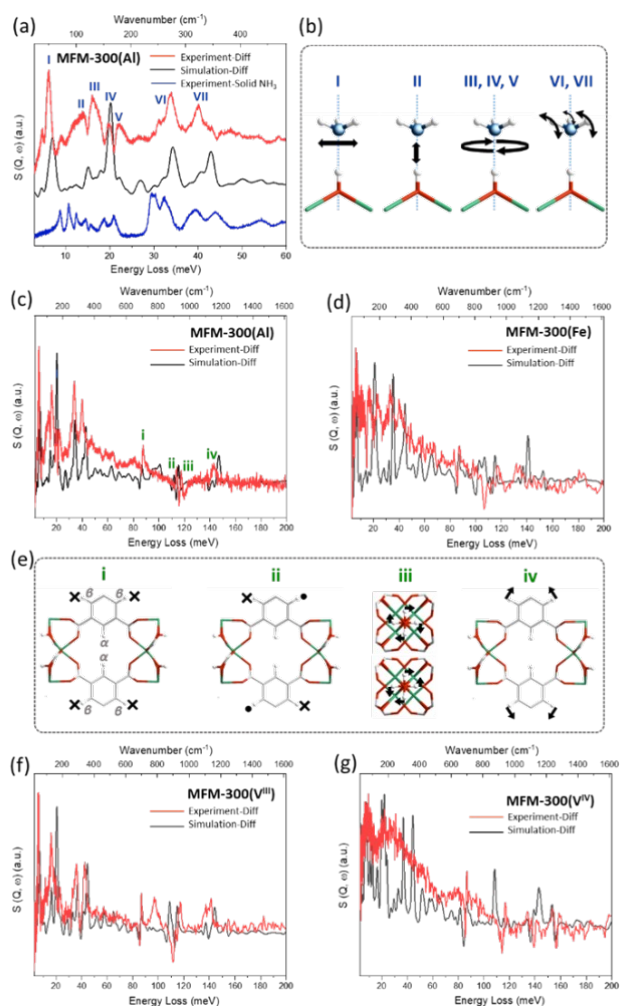


**Figure 5.** Comparisons of the experimental (red) and DFT-simulated (black) difference INS spectra of bare and  $\text{NH}_3$ -loaded MFM-300; (a) direct comparison with condensed  $\text{NH}_3$  in the solid; (b), (e) vibrational modes of adsorbed  $\text{NH}_3$  and of MFM-300(Al) host; (c), (d), (f), (g): difference INS spectra for  $\text{NH}_3$  in MFM-300(M) (M = Al, Fe,  $\text{V}^{\text{III}}$ ,  $\text{V}^{\text{IV}}$ ), respectively.



**Table 1.** Summary of NH<sub>3</sub> adsorption in MFM-300 materials

| MFM-300(M)   | M = Al          | M = V <sup>III</sup> | M = V <sup>IV</sup> | M = Cr          | M = Fe          |
|--|-----------------|----------------------|---------------------|-----------------|-----------------|
| Uptake capacity <sup>a</sup> (mmol/g)  | 15.7            | 15.6                 | 17.3                | 14.0            | 16.1            |
| NH <sub>3</sub> Storage density in MOFs <sup>a</sup> (g/cm <sup>3</sup> )      | 0.28            | 0.29                 | 0.34                | 0.27            | 0.30            |
| NH <sub>3</sub> Packing density in MOF pores <sup>a</sup> (g/cm <sup>3</sup> ) | 0.72            | 0.54                 | 0.61                | 0.51            | 0.60            |
| NH <sub>3</sub> Packing density in MOF pores <sup>b</sup> (g/cm <sup>3</sup> ) | 0.60            | 0.47                 | 0.53                | 0.44            | 0.52            |
| Pore Volume of MOF (cm <sup>3</sup> /g)  | 0.37            | 0.49                 | 0.48                | 0.47            | 0.46            |
| Surface area (m <sup>2</sup> /g)   | 1325            | 1755                 | 1719                | 1683            | 1647            |
| Enthalpy of adsorption (kJ/mol)  | 30 to 50        | 35 to 45             | 30 to 60            | 35 to 65        | 35 to 40        |
| Entropy of adsorption [J/(mol·K)]  | -240 to<br>-135 | -215 to<br>-150      | -240 to<br>-180     | -290 to<br>-210 | -215 to<br>-175 |

<sup>a</sup>: at 273K 1 bar;

<sup>b</sup>: at 298K 1 bar.

